PNNL-24726

Pacific Northwest
NATIONAL LABORATORY
Proudly Operated by Battelle Since 1965

Active Time-Domain Reflectometry for Unattended Safeguards Systems: FY15 Report

September 2015

JR Tedeschi
LE Smith
DE Moore
DM Sheen
RC Conrad
G Gavric

U.S. DEPARTMENT OF ENERGY

Prepared for the U.S. Department of Energy
under Contract DE-AC05-76RL01830

DISCLAIMER

PACIFIC NORTHWEST NATIONAL LABORATORY
operated by
BATTELLE
for the
UNITED STATES DEPARTMENT OF ENERGY
under Contract DE-AC05-76RL01830

Printed in the United States of America

Available to DOE and DOE contractors from the
Office of Scientific and Technical Information,
P.O. Box 62, Oak Ridge, TN 37831-0062;
ph: (865) 576-8401
fax: (865) 576-5728
email: reports@adonis.osti.gov

Available to the public from the National Technical Information Service,
U.S. Department of Commerce, 5285 Port Royal Rd., Springfield, VA 22161
ph: (800) 553-6847
fax: (703) 605-6900
email: orders@ntis.fedworld.gov
online ordering: http://www.ntis.gov/ordering.htm

This document was printed on recycled paper.
(9/2003)

PNNL-24726

Active Time-Domain Reflectometry for Unattended Safeguards Systems: FY15 Report

JR Tedeschi
LE Smith
DE Moore
DM Sheen
RC Conrad
G Gavric

September 2015

Prepared for
the U.S. Department of Energy
under Contract DE-AC05-76RL01830

Pacific Northwest National Laboratory
Richland, Washington 99352

Abstract

The International Atomic Energy Agency (IAEA) continues to expand its use of unattended measurement systems. An increasing number of systems and an expanding family of instruments create challenges in terms of deployment efficiency and the implementation of data authentication measures. In collaboration with the IAEA, tamper-indicating measures to address data-transmission authentication challenges with unattended safeguards systems are under investigation. Pacific Northwest National Laboratory (PNNL) is studying the viability of active time-domain reflectometry (TDR) along two parallel but interconnected paths: (1) swept-frequency TDR as the highly flexible, laboratory gold standard to which field-deployable options can be compared, and (2) a low-cost commercially available spread-spectrum TDR technology as one option for field implementation. This report describes PNNL's FY15 progress in the viability study including: an overview of the TDR methods under investigation; description of the testing configurations and mock tampering scenarios; results from a preliminary sensitivity comparison of the two TDR methods; demonstration of a quantitative metric for estimating field performance that acknowledges the need for high detection probability while minimizing false alarms. FY15 progress reported here sets the stage for a rigorous comparison of the candidate TDR methods, over a range of deployment scenarios and perturbing effects typical of IAEA unattended monitoring systems.

Acknowledgments

This research was supported by the U.S. National Nuclear Security Administration (NNSA) Office of Nonproliferation and International Security (NA-24), and its Next Generation Safeguards Initiative, under Contract DE-AC05-76RL01830 with the U.S. Department of Energy. Pacific Northwest National Laboratory is a multi-program national laboratory operated by Battelle for the U.S. Department of Energy. The authors would also like to thank Jeff Sanders, Benjamin Baker, John Svoboda and Jim West from INL, and Kiril Ianakiev from LANL, for their collaboration and technical discussions on the topic of tamper-indicating methods for IAEA's unattended monitoring systems. We would also like to thank Roman Simlinger and Cesare Liguori of the IAEA for their collaboration on LiveWire implementation options.

Acronyms and Abbreviations

ASIC	application specific integrated circuit
BPSK	binary phase shift keyed
DSSS	direct sequence spread spectrum
DUT	device under test
EMI	electromagnetic interference
FAR	false alarm rate
FEE	front-end electronics
HPF	high pass filter
IAEA	International Atomic Energy Agency
INL	Idaho National Laboratory
LANL	Los Alamos National Laboratory
LPF	low pass filter
NGSI	Next Generation Safeguards Initiative
PCB	custom printed circuit board
PD	probability of detection
PNNL	Pacific Northwest National Laboratory
PTFE	polytetrafluoroethylene
ROC	receiver operating characteristic
SMA	sub-miniature version A
SSTDR	spread spectrum time domain reflectometry
TDR	time domain reflectometry
TI	tamper-indicating
UMS	unattended monitoring system
VNA	vector network analyzer

Contents

Figures

Tables

1.0 Introduction

Remotely monitored, unattended nondestructive assay systems are central to the International Atomic Energy Agency's (IAEA's) ability to safeguard an expanding global fuel cycle with limited manpower and financial resources. As the number of unattended monitoring instruments increases, the IAEA is challenged to become more efficient in the implementation of those systems, and to ensure the authenticity of data coming from an expanding family of instruments. Ensuring that the detector signals received at the IAEA cabinet are authentic is central to the independence of IAEA's safeguards conclusions. Unfortunately, traditional data security measures, for example tamper-indicating conduit, are impractical for the long separation distances (often 100 m or more) between unattended monitoring system (UMS) components. Challenges include the fact that such conduit requires detailed physical inspection by the IAEA during on-site visits, and often, the cabling is routed through multiple penetrations in difficult-to-access parts of the facility. These inspections are tedious, time-consuming, and only periodic, rather than continuous. Advanced tamper-indication (TI) options are needed, and the *IAEA Department of Safeguards Long-Term R&D Plan, 2012-2023* identifies this need for the "ability to communicate secure, authentic information…between the IAEA…and equipment in the field" [9].

2.0 Background

Under support from the U.S. National Nuclear Security Administration's Next Generation Safeguards Initiative (NGSI), a multi-organization collaboration of Pacific Northwest National Laboratory (PNNL) (lead), Idaho National Laboratory (INL), and Los Alamos National Laboratory (LANL) is studying candidate TI methods for IAEA's unattended monitoring systems. The collaborators are performing independent investigations of different candidate TI approaches: active time-domain reflectometry (PNNL), passive noise analysis (INL), and pulse-by-pulse analysis and correction of signal integrity (LANL). Among the development questions to be addressed in the project are:

- How do the fundamental characteristics of these TI candidate methods differ?
- Can TI signals be distinct and separable from the frequency spectra of common UMS sensor types?
- How effectively can the candidate methods detect common tampering scenarios?
- Are there obvious vulnerabilities in the methods and, if so, how might they be addressed?
- For promising TI methods, what are the implementation options? How might they interface with common IAEA data acquisition systems?

The project team developed two use cases, representative of IAEA UMS deployments today and the in the future, to guide the study:

Use Case 1: Retrofit of advanced TI methods into existing deployments where the sensor is co-located with the front-end electronics (FEE) (Figure 1). This is the highest priority use case because it is how the vast majority of IAEA systems are deployed today.

Use Case 2: Integration of advanced TI methods in deployments where the FEE is separated from the sensor, creating two distinct sections of cabling, one between the sensor and the FEE, and the other between the FEE and the IAEA cabinet (Figure 2).

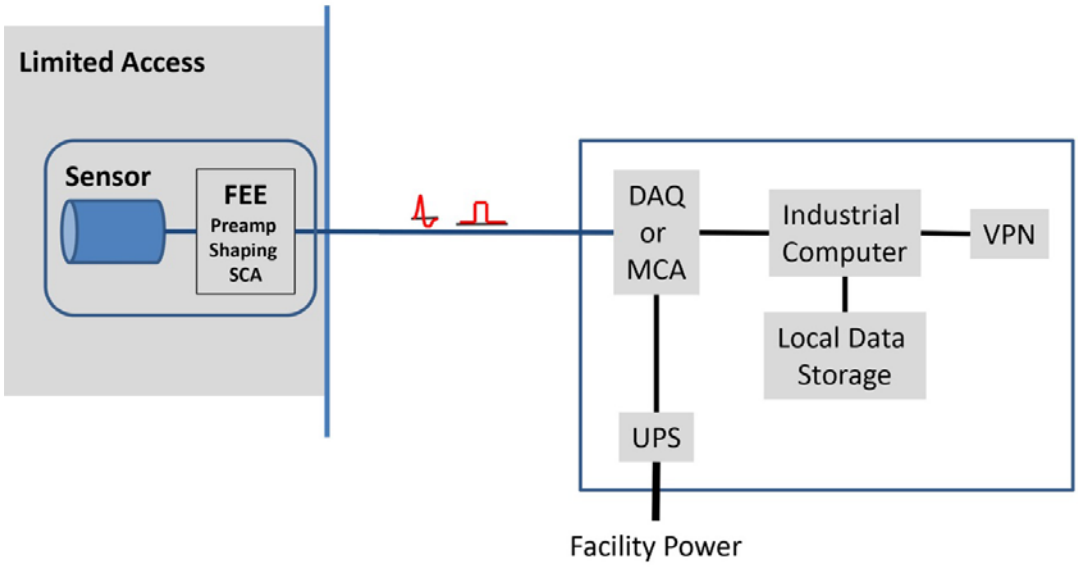

Figure 1. Use Case 1, FEEs are co-located with the sensors, often inside an area of limited personnel access.

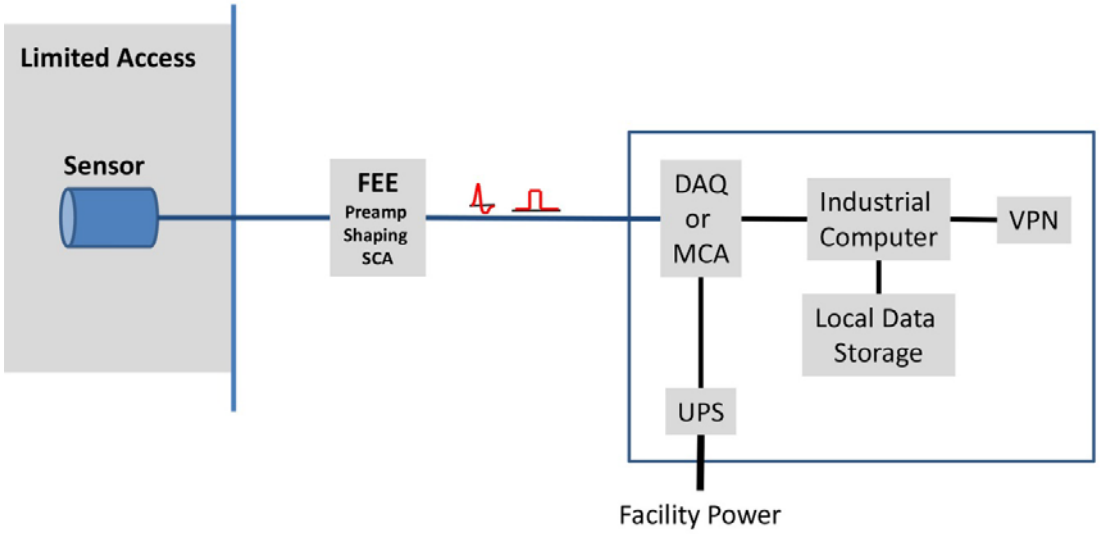

Figure 2. Use Case 2, FEEs are separated from the sensor and the cabinet.

It is assumed in this study that the baseline, unperturbed condition of the cabling is verified and known upon initial installation of the UMS cabling and equipment so that TI methods for physical intrusion are focused on detecting *changes* in the cabling characteristics from that baseline. Note that while these use cases are illustrated above with a single sensor and FEE, typical IAEA deployments involve multiple sensors and multiple cables.

The NGSI study is framed by two distinct tampering scenarios: (1) physical intrusion into the cabling, and (2) signal tampering (e.g., the injection of synthetic signals that emulate real signals under normal operational conditions). For either tampering scenario, the TI method should raise a flag to indicate that

the instrumentation system may have been compromised and, therefore, that safeguards data produced by that instrument from that time forward may be suspect.

To date, the IAEA has not issued formal requirements for new technologies intending to address these two TI challenges. To guide the NGSI study of candidate TI methods, the project team has developed preliminary functional requirements and performance targets for the first scenario: physical intrusion into cabling [3]. Cable tampering scenarios defined by the NGSI team include taps, splices, disconnects, and replacements. Metrics for evaluation of the candidate TI methods include detection probability and false-alarm rate under various operational conditions, ability to localize the tampering event, and the value of diagnostics provided by each method that could aid the IAEA in determining the likely cause of the tamper indication.

3.0 Candidate TDR Methods

PNNL's initial investigation of the viability of active time-domain reflectometry (TDR) for the detection of physical intrusion into cabling is taking two parallel but interconnected paths: (1) swept-frequency TDR (SFTDR) as the highly flexible, laboratory gold standard to which field-deployable options can be compared, and (2) a low-cost commercially available spread-spectrum TDR (SSTDR) technology as one option for field implementation. A brief description of each is provided below.

3.1 Swept-Frequency Time-Domain Reflectometry

The swept-frequency TDR measurement method is put to practice in this study using an Agilent Technologies Vector Network Analyzer (VNA). The VNA TDR uses Fourier analysis of swept frequency domain signals, velocity of signal propagation, and transmission line impedance changes to determine both amplitude and position in time/space of reflected signals. Figure 3 below shows the VNA with the cable under test connected to Port 1 of the network analyzer.

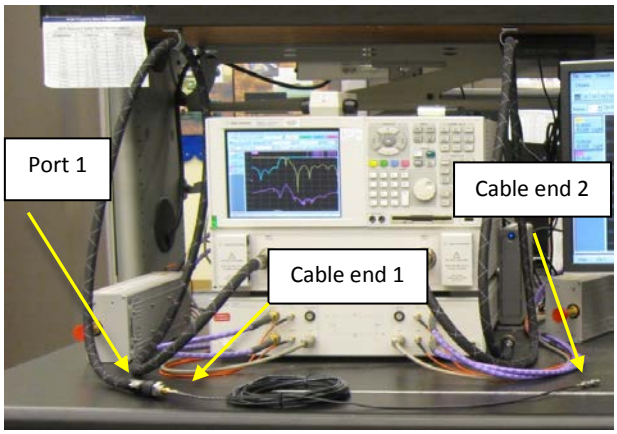

Figure 3. Keysight Technologies VNA with test cable connected to Port 1.

For a standard coaxial transmission line, the line impedance is expected to be nominally continuous throughout the cable; however, if the cable now connects to a device under test (DUT), there will be a reflection if the DUT impedance does not perfectly match the impedance of the coaxial line. The reflection coefficient is defined as follows:

$$\rho = \frac{Z_{DUT} - Z_0}{Z_{DUT} + Z_0},$$

where Z_0 is the transmission line impedance and Z_{DUT} is the impedance of the DUT. Performing an electronic calibration on the VNA [4] corrects for the insertion loss, impedance, and phase associated with the VNA and its test cables that connect the VNA to the DUT. Therefore, this allows the VNA to perform fully calibrated amplitude and phase frequency measurements that are in response to the DUT. The VNA then performs a swept frequency domain reflection measurement and mathematically computes a time domain transform using the chirp-Z Fast Fourier Transform technique [5]. The reflection or S11 measurement refers to the measured signal amplitude and phase received at Port 1 relative to the transmitted amplitude and phase from Port 1. The time domain data is then converted into the spatial domain by a second translation using signal phase velocity, also expressed as the velocity of light in the medium. The phase velocity for non-magnetic materials is determined using the equation shown below [6],

$$v_P = \frac{c}{\sqrt{\varepsilon_r}}$$

where c is the speed of light (3×10^8 m/s), and ε_r is the real part of the dielectric constant of the propagation medium. For reference, the phase velocity of in polyethylene and polytetrafluoroethylene (PTFE), are 66% and 69% of the phase velocity in free space respectively.

3.2 Spread-Spectrum TDR with LiveWire

SSTDR-LiveWire [7] was designed to operate continually in the background of a system to monitor for cable breaks and shorts without influencing the operation of the system being monitoring. LiveWire uses a spread spectrum TDR (SSTDR) technique with low-power signals that, when viewed in the frequency domain, appear as noise rather than continuous wave or swept continuous wave signals. For SSTDR to generate its ‘noise’ frequency range, a sine wave that has been shaped into a square wave is multiplied by a pseudo noise correlator; this generates a direct sequence spread spectrum (DSSS) binary phase shift keyed (BPSK) signal [8]. This DSSS BPSK signal is then mixed with the original sine wave to produce a spread-frequency spectrum signal that is injected into the cable. Figure 4 presents an example of a sine wave being BPSK modulated.

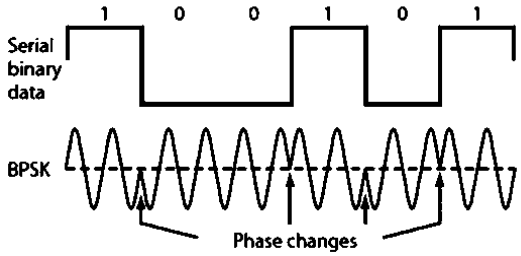

Figure 4. Sine wave BPSK modulated signal time domain response.

The return signal, after reflection from discontinuities in the transmission path, includes any added noise or other frequency content from the system being monitored. The reference signal is the original sine wave with a variable phase delay applied; adjusting the phase delay allows for localization of the discontinuities in the cable. The reflected signal is cross-correlated with a reference signal to determine the location of the discontinuity.

LiveWire implements their SSTDR method in a number of form factors but in this study, the primary focus is a small, low power, portable application specific integrated circuit (ASIC). The design of the ASIC is tailored to the detection of faults, either open or shorts, on power or communication networks without causing any disturbances of its own. A primary user of the device to date has been the aircraft industry. This stand-alone package can be customized for specific uses, and is the device that has been of interest to the IAEA.

In 2010, the IAEA began an investigation of the LiveWire TDR method for applicability in both surveillance and unattended radiation detection systems. The very early proof-of-concept tests performed by the IAEA and a LiveWire representative were inconclusive but encouraging. The IAEA continued its study of LiveWire with a focus on surveillance applications using analog cameras (e.g., radiation-hardened cameras). IAEA staff purchased a LiveWire ASIC, designed and fabricated printed circuit boards (PCBs) to support the ASIC and the accompanying microcontroller, and developed a software interface to support testing. By 2013, those tests were sufficiently successful to support a dedicated integration effort for IAEA surveillance needs. A project under the German Support Program to the IAEA is now underway to integrate the LiveWire ASIC in the controller module for one of the IAEA analog camera systems.[(a)]

While the IAEA's study of LiveWire for surveillance has proceeded significantly in recent years, there has been no corresponding progress on its viability for unattended radiation detection systems. PNNL, in the course of its TDR investigation in the NGSI project, is positioned to inform the IAEA on this topic. In recognition of this opportunity, the IAEA provided (in October 2014) sample implementations of its PCBs, microcontroller, and software to PNNL as the start of a collaborative investigation on LiveWire for IAEA UMS.

Building from the IAEA-provided foundation, PNNL developed a LiveWire evaluation platform that includes the LiveWire ASIC and an Arduino Due microcontroller (Figure 5). The Arduino provides user

([a]) Roman Simmlinger, International Atomic Energy Agency, personal communication, 2014.

control and interface with the LiveWire ASIC via a C# graphical user interface (GUI) on a desktop PC. The output from the LiveWire ASIC connects to a SubMiniature version A (SMA) female bulkhead adapter where the cable under test connects. The output from the LiveWire ASIC is read by the Arduino and uploaded to the host computer where the data is processed and stored as comma separated value files. The raw data are analyzed, offline, using data reduction and algorithms developed by PNNL using Matlab™.

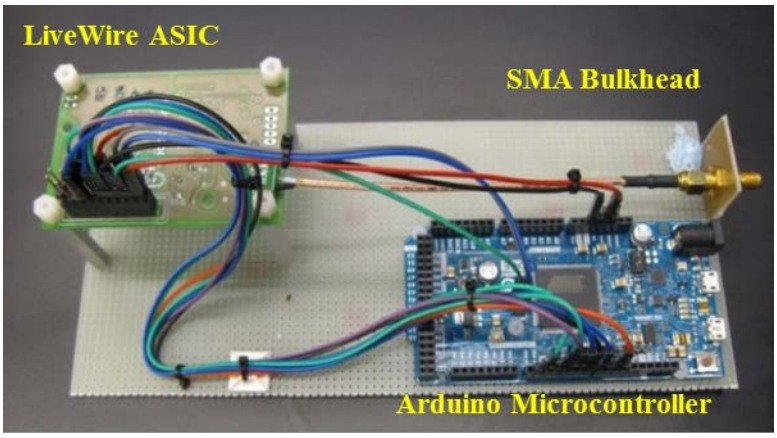

Figure 5. PNNL's prototype SSTDR system based on LiveWire's ASIC.

4.0 Testing Configurations

In testing to date, the range of tampering scenarios identified by the NGSI Team [1] have been approximated through a combination of attenuator variation at the end of the cable, and destructive physical intrusion in the cabling itself. PNNL has defined and utilized two test configurations (Figure 6) with respect to Use Case #1 previously shown in Figure 1. Test configuration #1 connects the TDR system under test to Port 1 of the cable under test, while the other end of the cable is connected to various attenuation values. This configuration allows investigation of how effectively a TDR system can detect the device impedances represented by the attenuators, without regard for the radiation-detector signals propagating through the cable. In addition to the attenuator tests, physical tampering is performed on the cable under test at three locations on the line: 25m, 37.5m, and 50m.

Test configuration #2 supports investigation of a more realistic scenario in which a signal representative of the radiation detectors employed by the IAEA is propagating through the cable during the TDR measurement. This configuration includes a representative UMS bipolar pulse supplied by an arbitrary waveform generator (AWG) connected to the second port of the cable under test, emitting a single cycle of a sine wave with a frequency of 3.33MHz repeated every 100usec.

RG174 is a common cabling type for IAEA deployments and has been the focus of initial studies. RG174's electrical specifications are: impedance 50Ω +/- 5Ω (10MHz-3GHz), conductor resistance 142.6Ω/km, attenuation 0.36dB/m at 100MHz, 1.18dB/m at 1GHz, and 2.1dB/m at 3GHz [10].

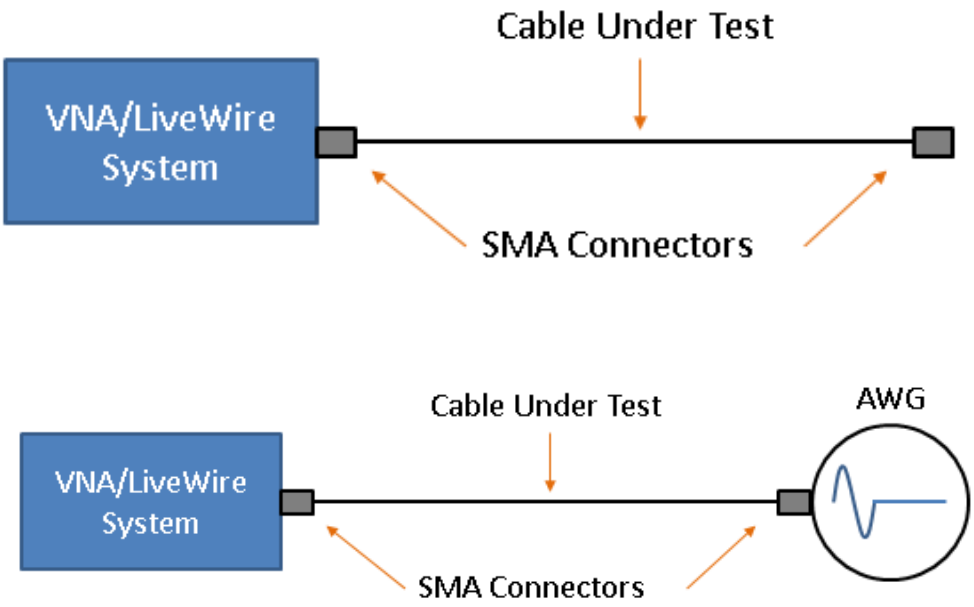

Figure 6. Test configuration #1 (top) and #2 (bottom). The AWG represents a radiation detector; 50m of RG 174 cabling is used.

Comparison of results and findings from these two configurations supports quantitative investigation into the detection sensitivity of the TDR systems and effects of the radiation detector signal on the TDR performance. For each configuration and each TDR method, a baseline, reference measurement was collected prior to any impedance changes or tampering. The baseline response allows for baseline subtraction, predetermining the noise floor levels, and identifying the unique electrical structure of the cable prior to destructive testing. The baseline response is central to the type of "relative" analysis methods envisioned for TDR implementations for unattended radiation-detection systems.

4.1 Attenuator Variation

For the attenuator variation studies (test configuration #1), the reflection difference in dB from an open circuit at the end of the cable to the case with the attenuator preceding the open circuit is equal to twice the attenuator value, as we are measuring a reflected signal that passes through the attenuator on the way to the open and then back through the attenuator once it reflects. The dB reduction from the reflection at the end of the cable can be correlated to representative impedance by using the formula for calculating the reflection S-parameter, S11, based upon the device under test (DUT) and the impedance of the line.

$$S11_{dB} = 20\log\left(\frac{Z_{DUT} - Z_O}{Z_{DUT} + Z_O}\right)$$

Since we know the impedance of our line, Z_0, is 50ohms, and the reflection coefficient from an open will be 0dB (pure reflection). Therefore the reflection response from an attenuator preceding the open circuit will be 0dB – 2*(attenuator value). So the higher the attenuator value the more the reflection from the open will begin to look like a 50ohm response. Solving for the impedance of the DUT produces the following equation.

$$Z_{DUT} = Z_O\left(\frac{1+10^{((0-2*Attn)/20)}}{1-10^{((0-2*Attn)/20)}}\right)$$

Figure 7 below shows the calculated representative impedance curve that the attenuators present to our measurement systems with an open at the end of the cable. Table 1 calls out the specific attenuation values used in this measurement study and their representative device impedance.

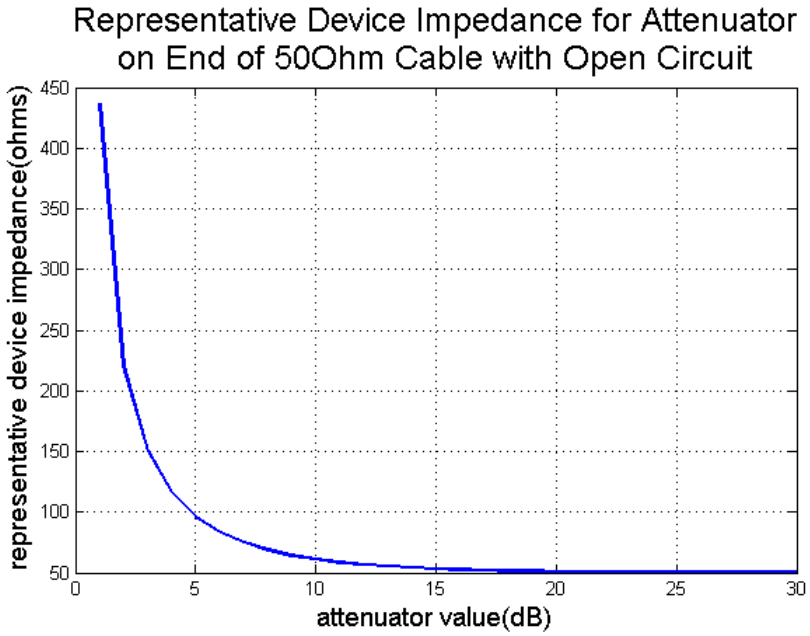

Figure 7. Attenuator representative impedance curve at the end of an open cable.

Table 1. Attenuator value vs. representative device impedance

Attenuator Value	Representative Impedance Change
1	436.2116
2	220.9714
3	150.476
6	83.545
8	68.8339
9	64.4024
10	61.1111
20	51.0101
30	50.1001

4.2 Physical Intrusion

Cable physical intrusion scenarios involved a cut in the jacket of the RG174 cable, from which the braided shield was peeled back in a 2mm x 2mm area to provide enough space for a 10MΩ high impedance probe to press through the dielectric and make contact with the center conductor (without shorting to the braided shield). The ground reference was then clamped onto the outer conductor that had been peeled back, see figures 8 and 9. The validity of the tamper was confirmed by injecting a sine wave on the RG174 cable and verifying that the signal could indeed be collected by the probe without shorting the line (which would cause a large reflection for the TDR systems).

Figure 8. Physical tamper in RG174 cable.

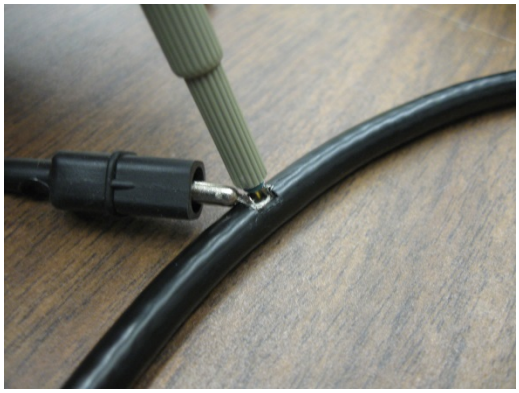

Figure 9. Tamper with high impedance probe and ground reference installed.

4.3 TDR Parameter Settings

A series of scoping measurements were performed with both the VNA and Livewire in order to determine reasonable parameter settings for the initial comparative studies to be performed in FY15. The key parameters, including transmission bandwidth, power, and sweep time were selected in order to increase sensitivity to impedance changes and tampers, while maintaining a low signal transmission power and < 1sec data collection. It is important to note that these parameter settings have not been optimized; they merely provide a nominal starting point for future optimization studies.

For the VNA system, the selected transmission bandwidth was 50-3050MHz. This bandwidth was sufficient to provide reduced attenuation effects in the RG174 but wide enough to provide sharp downrange spatial resolution. Downrange spatial resolution refers to the ability to resolve two distinct reflection peaks. That minimum resolvable separation is inversely related to the bandwidth, so that wider bandwidths generally translate to improved downrange resolution. The transmission power selected was -5dBm or 355mVpp. The sweep time for a VNA is set by a few parameters: the number of points which determines frequency increment, and the intermediate frequency (IF) bandwidth; having a wide IF bandwidth provides for fast sweeps but also raises the system noise floor thereby reducing dynamic range. Therefore a VNA IF bandwidth of 5KHz was selected to provide a good balance of speed vs. sensitivity.

For the Livewire system, the frequency range of the selected pseudo noise spectrum generated by the BPSK modulation was from 12MHz – 36MHz. The transmission power level was 128mVpp. The Livewire system was limited in the number of frequency samples it could make during a single measurement, this however translated to very short measurement times. These short measurement times allowed for averaging of the data sets collected; 200 scans would be performed, averaged, and then saved as the reflected signal response.

5.0 Results

Examples of results from FY15 measurements are provided below. These results are presented in two forms. The first is a semi-quantitative comparison of sensitivity to conditions representative of intrusion scenarios. For these tests, sensitivity is estimated using a one-time measurement of the TDR signal and a comparison of that signal to a reference (baseline) signal. This provides an indication of the signal contrast achievable with each method. The second plotting method discussed in section 6.0 provides insight into how the system sensitivity translates to real-world field performance in which the key performance metric is the probability of detection (PD) for a given intrusion scenario and the false alarm rate (FAR) that must be tolerated to achieve that detection probability. The tradeoffs between PD and FAR are often quantified using Receiver-Operator Characteristic (ROC) analysis and this metric has been adopted for this study.

The analysis results presented below correspond to only a subset of the measurements performed in FY15. A complete list of measurements, not all of which were analyzed fully, is shown in Appendix A.

5.1 Semi-Quantitative Sensitivity Comparison

5.1.1 VNA SFTDR

Figure 10 shows the full measurement span in the spatial domain for the different impedances at the end of the 50m RG174 cable. Note the linear behavior of the S11 response up to a distance of 30m, due to insertion losses in the cable. Beyond 30m, the insertion loss of the cable is so great that the response becomes limited by the thermal noise floor of the VNA, resulting in a flattening of the response through 50m. Figure 11 provides additional detail on the 50-m range of most interest. It is important to note that responses in the measurement window shown past 50m are due to receiver noise or multipath reflections that produce responses later time/distance than the physical end of the cable under test.

The short and open-circuit have the same magnitude, as expected, while the 20dB and 30dB attenuators are quite similar to the 50-ohm termination (baseline) case. The 20dB attenuator represents a 51Ω impedance; the 30dB attenuator 50.1Ω. The 10dB attenuator at the end of the cable is clearly distinguished. Inferring from the 10dB response, in which there is approximately 5-10dB of dynamic range beyond the baseline, therefore a 15dB attenuator representative of 53.3Ω should also be distinguishable from the baseline case.

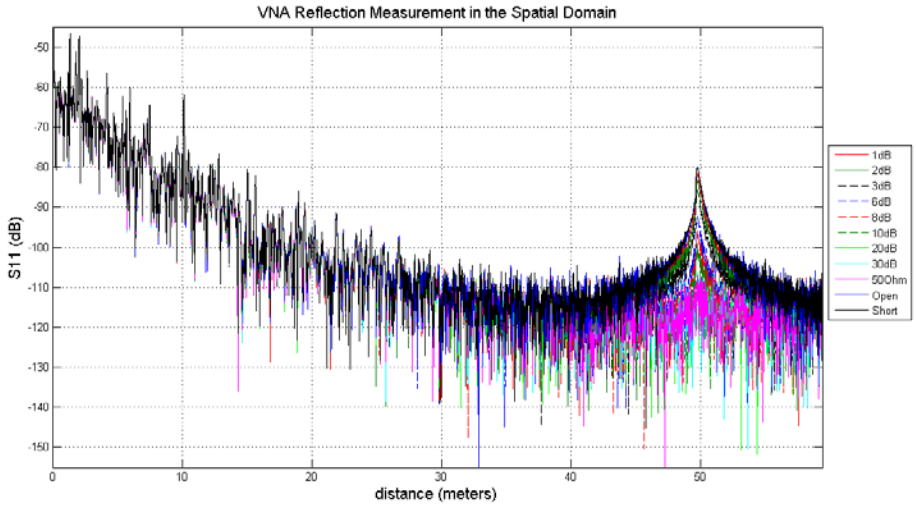

Figure 10. VNA responses from a single swept-frequency measurement for a range of attenuators installed at the end of the 50m cable (test configuration #1), wide downrange.

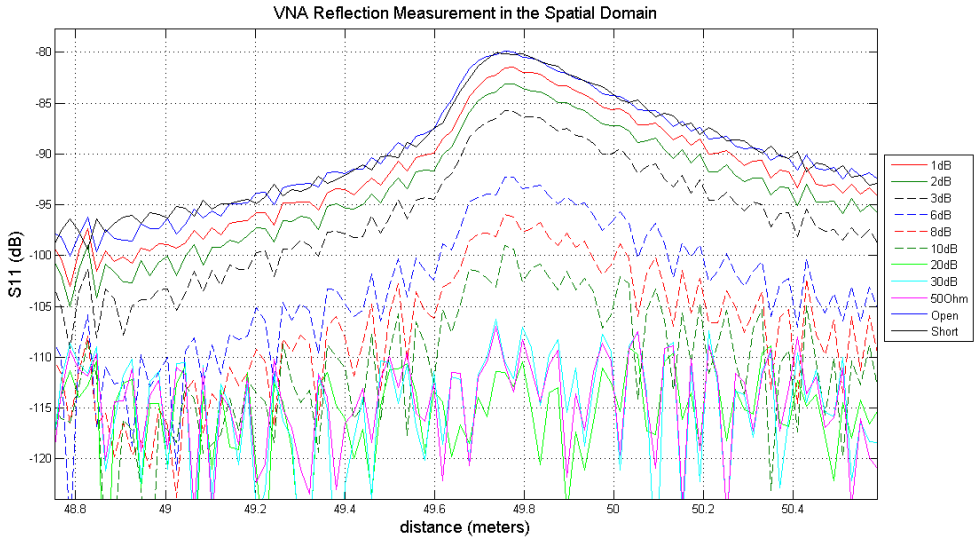

Figure 11. VNA responses from a single swept-frequency measurement for a range of attenuators installed at the end of the 50m cable (test configuration #1), narrow downrange.

The second set of VNA results are also from test configuration #1 but with physical tampers made on the cable line in three locations (Figure 12). Note that in each measurement, the high-impedance probe was only installed at the location for the tamper under test, i.e., for the 25-m case, the high impedance probe was installed at that location, not in the 37.5-m and 50-m locations. The VNA response to physical

tampers at 25m and 37.5m is clearly distinguishable from the baseline, but the response at 50m is significantly less prominent due to interference from cable-end reflection features.

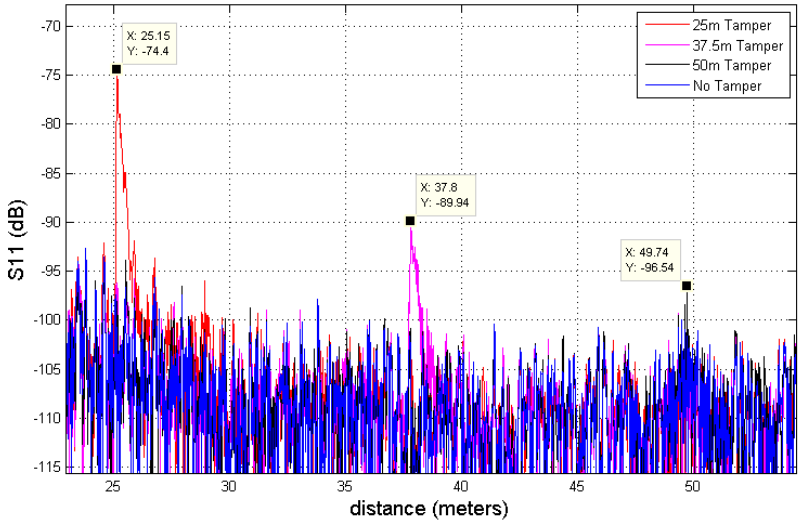

Figure 12. VNA responses from a single swept-frequency measurement, for physical tampers at various locations in test configuration #1 (50-ohm termination installed at end of cable).

The physical tamper study was repeated with test configuration #2, in which the AWG was installed at the end of the coaxial cable, rather than a 50-ohm termination. The results, shown in Figure 13, were qualitatively identical to Figure 12 indicating that the single-impulse sine wave from the AWG does not significantly impact the VNA TDR signal. This is the expected result due to the incoherence of the VNA sweep and the AWG signal, and also the bandwidth separation between the VNA, 50-3050MHz, and the AWG, 3.33MHz. While the VNA presented encouraging initial results, significantly more investigation into potential interference effects between VNA and radiation-detector signals is needed.

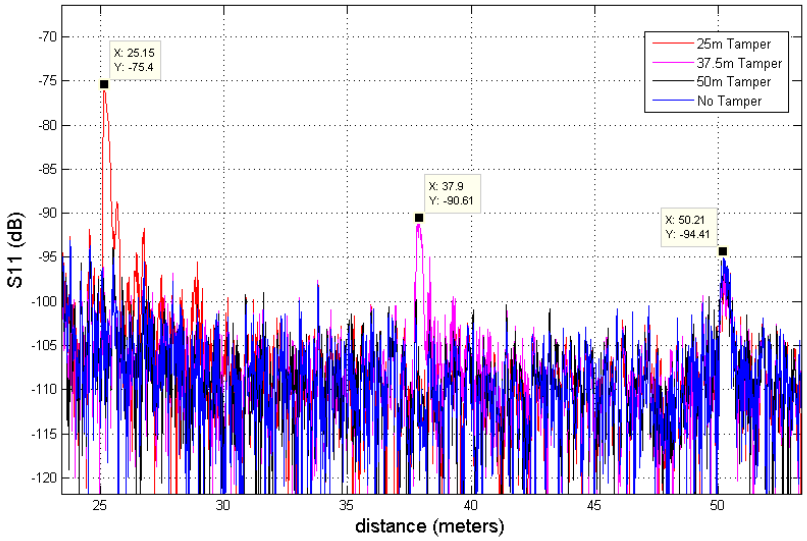

Figure 13. VNA responses from a single swept-frequency measurement for physical tampers at various locations and test configuration #2 (AWG at end of cable, transmitting a signal representative of radiation detectors).

5.1.2 Livewire SSTDR

The LiveWire SSTDR system was tested in the same measurement configurations as the VNA, with initial operating parameters intended to maintain high sensitivity to small impedance variations, while reducing EMI/noise effects and ensuring that the LiveWire signal is sufficiently low to avoid interference with the radiation detectors signals. The Livewire system is more rigid in terms of its bandwidth, output power, etc., but it has the advantage in that it can perform a complete measurement very quickly, on the order of microseconds. This allows for averaging of the measured responses and a reduction in noise and electromagnetic interference (EMI) effects. The initial parameters for the LiveWire system were selected in order to detect small impedance variations, reduce EMI/noise effects, and keep the Livewire signal at a low amplitude level to minimize potential interference with the radiation detectors signal. The selected parameters are as follows: 1) bandwidth: 24MHz (fc nominally 12MHz), 2) output power: 128mV, 3) averaged waveforms: 200.

The preliminary results in Figure 14 show the SSTDR reflections for a range of attenuators in test configuration #1. Note that the response from an open-circuit versus a short-circuit condition produces the same magnitude but an inverted response, due to the sign change in the S11 equation with a DUT impedance of zero versus a DUT impedance of infinity.

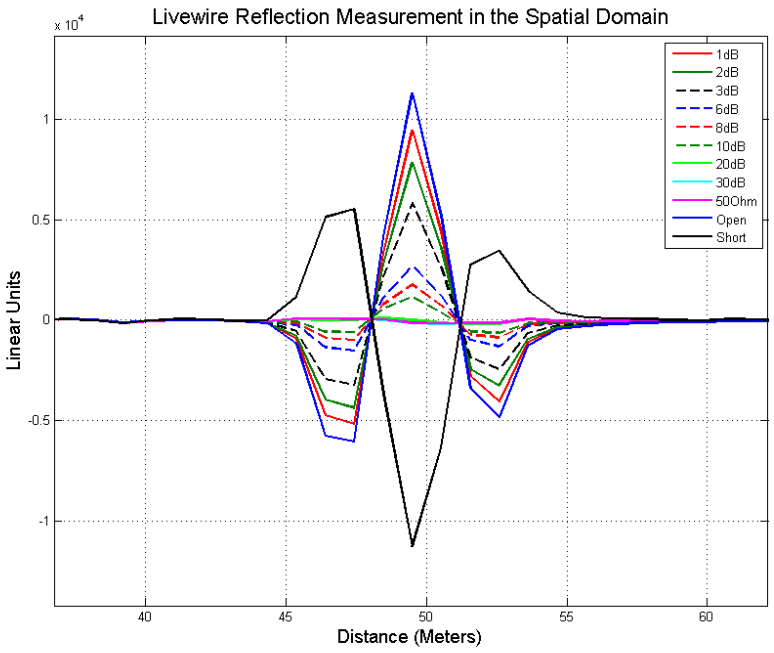

Figure 14. LiveWire signals for a range of attenuators installed at the end of the 50m cable (test configuration #1).

The LiveWire system was then tested with the same physical tampers used for the VNA system, in test configuration #1. As with the VNA results, the LiveWire signals were easily separable from the baseline response for tampers at 25m and 37.5m, but the 50-m intrusion was much less prominent (Figure 15). For the 25m and 37.5m cases there were 23.2dB and 18.7dB deltas respectively from the baseline. At 50m there is little to no difference from the baseline, for these specific scan parameters. Note that there is a reflection response structure at 50m, most likely due to an imperfect match between the 50-ohm

termination and the cable impedance, and this structure may be masking the tamper reflection at 50m. PNNL is considering implementation approaches (e.g., short length of extra cabling in the tamper-indicating enclosure) that would mitigate such masking.

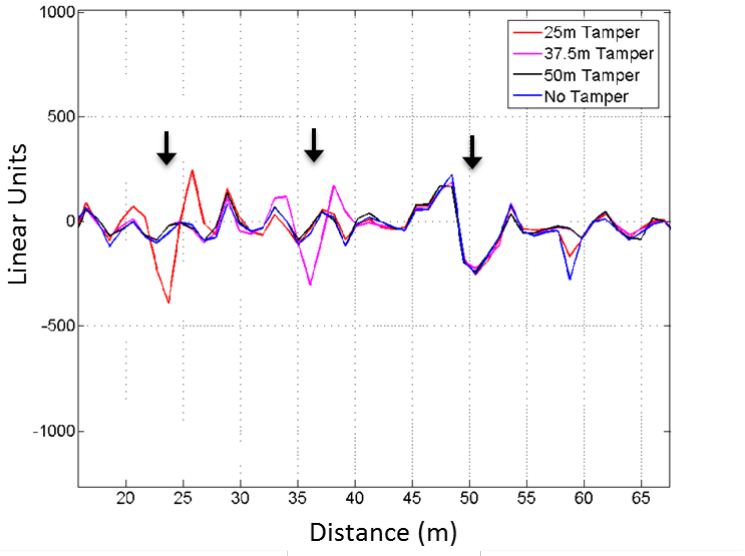

Figure 15. LiveWire responses for physical tampers at various locations (black arrows) and test configuration #1 (50-ohm termination installed at end of cable).

The tamper test was then repeated with an AWG at the end of the 50-m cable rather than a 50-ohm termination. The AWG presented the same single-cycle sine wave pulse as described previously for test configuration #2. It was observed that since the AWG signal is not coherent with the LiveWire signal its interference was random and mitigated using the multi-scan averaging process. Further investigation on potential interference between LiveWire and radiation-detector signals is ongoing.

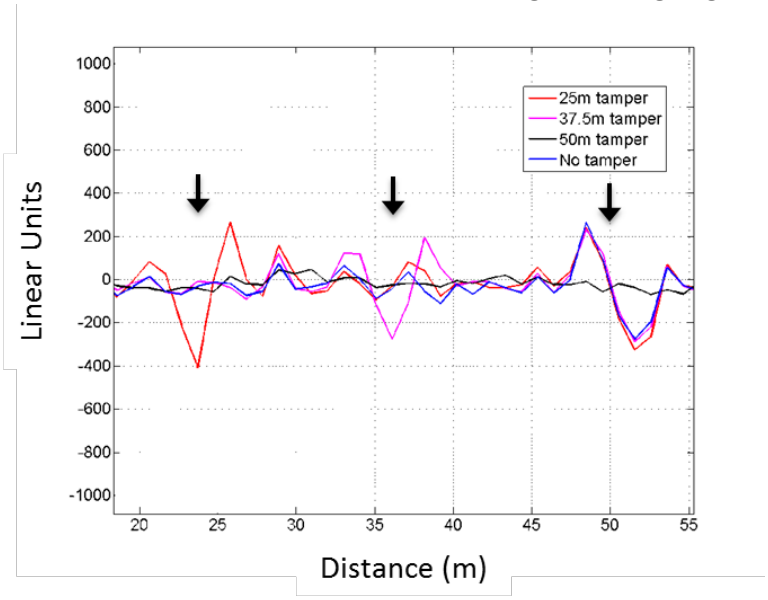

Figure 16. LiveWire responses for physical tampers at various locations and test configuration #2 (AWG at end of cable, transmitting a signal representative of radiation detectors).

5.1.3 Preliminary Sensitivity Comparison

A preliminary comparison of the VNA (SFTDR) and LiveWire (SSTDR) results for the range of attenuators examined in test configuration #1 is given in Figure 17. Figure 17 displays the differential magnitude in dB between the measurements with 50-ohm terminations at the end of the 50-m cable (baseline measurements) and the measurements with attenuators installed or physical tampering for both the VNA and LiveWire systems.

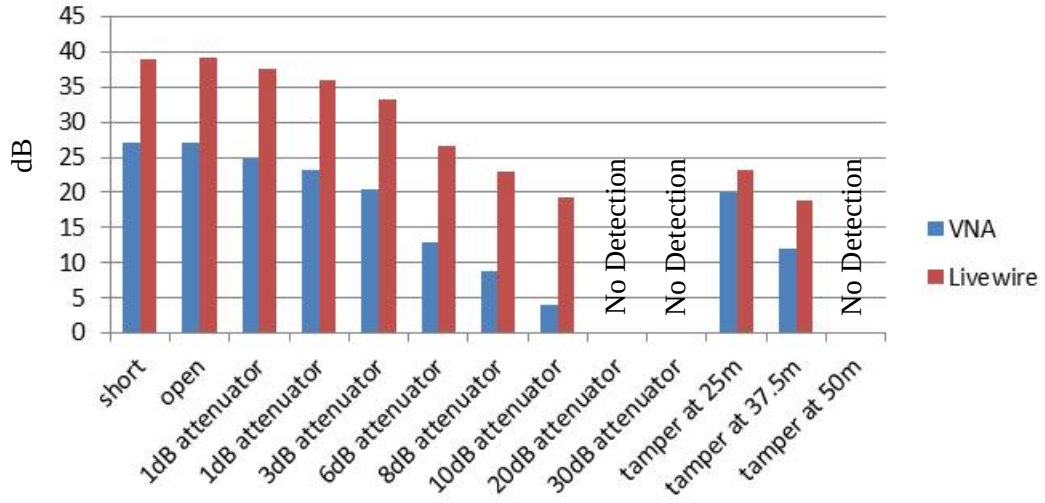

Figure 17. Comparison of VNA and LiveWire responses, in terms of differential amplitude (in dB) from a baseline signal, for a range of attenuators in test configuration #1.

6.0 ROC Curve Analysis as Predictor of Field Performance

The sensitivity comparison described above is a necessary and useful first step in understanding the potential of the candidate TDR methods, but such analysis does not translate directly into how TDR methods will actually perform in field implementation where the key variables of interest are the probability of detecting a tamper, and the corresponding false alarm rate. As described previously, ROC curve analysis methods can be used to map the relationship between PD and FAR for various tamper-detection scenarios defined, for example, by the type of tamper, electromagnetic background, radiation sensor type, etc.

In FY15, PNNL developed ROC analysis methods and exercised them on a subset of the LiveWire TDR data. The primary goal of this effort was to demonstrate an initial TDR analysis toolbox that can evaluate candidate methods in a way that moves beyond isolated benchtop experiments and speaks directly to anticipated field performance.

For tamper-indication studies, ROC analyses are based on two large sample populations: 1) baseline (no-tamper) samples and, 2) tampered. A sample is defined as one scan of the cable. In the FY15 case study, the baseline and tampered populations each consisted of 10,000 samples. That is, the baseline population consisted of 10,000 scans of a 50-m cable with no tamper installed; the tampered population was collected using a tamper inserted at 25m in that same cable. The measured scan responses from each

sample were analyzed using algorithms developed by PNNL in Matlab™. In FY15, the analysis algorithm was relatively simple: select the maximum signal intensity over the duration of the scan response (Figure 18). A histogram of these maxima was created for each of the sample populations. FAR was calculated by recording the fraction of the baseline histogram above a specific threshold on signal intensity. PD was calculated similarly, using the fraction of the tampered histogram above the threshold at the tamper location. For cases where the baseline and tampered histograms are well-separated, high PD can be achieved at low FAR. For scenarios where the distributions overlap, high FAR must be tolerated to achieve high PD.

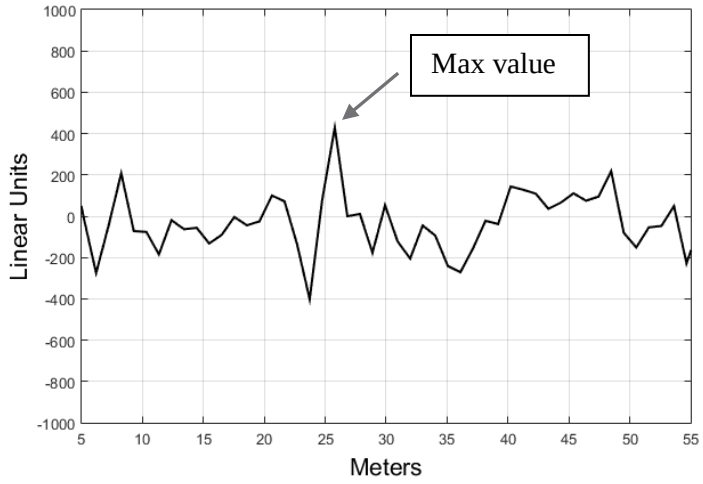

Figure 18. Example of maximum amplitude detection within 25m tamper sample.

The demonstration ROC analysis presented below was used to quantify the value of scan-signal averaging. Intuitively, it would be expected that averaging of multiple cable scan sequences would reduce the noise level and therefore, improve performance. Averaging more scan sequences may be required for tampers located further from the interrogating end of the cable, due to the attenuation losses described earlier. It is expected that averaging will reach diminishing returns at some point, however, as systematic uncertainties begin to dominate. Practical issues related to how many waveforms can be efficiently processed in field-deployed systems will also play a role. Example ROC results for LiveWire applied to a 50-m cable and tampering at 25m are shown below. The positive effects of averaging are easily observed in viewing histograms of the baseline and tampered populations, and the corresponding ROC curves Figures 19, 20 and 21 depict results for no averaging (i.e., single-scan), averaging over 25 scans for each sample of the population, and averaging over 200 scans respectively.

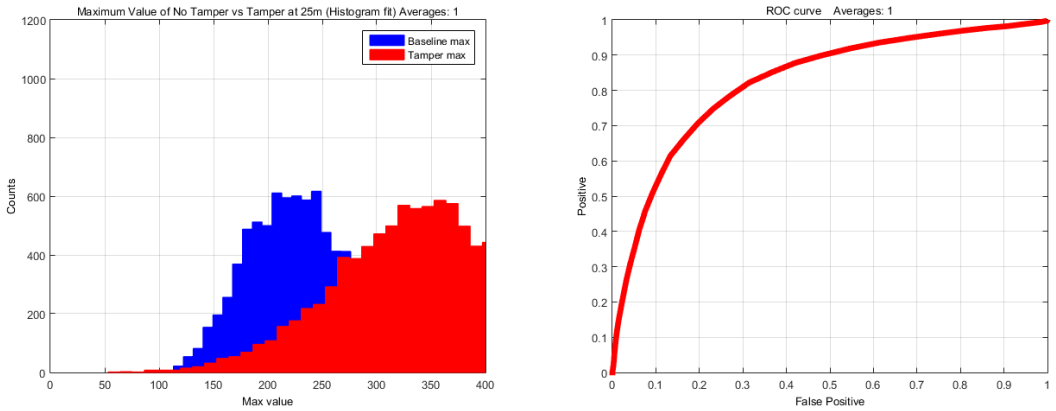

Figure 19. Baseline (blue) and tampered (red) populations (left) and corresponding ROC curve (right) assuming tamper at 25m and no scan averaging.

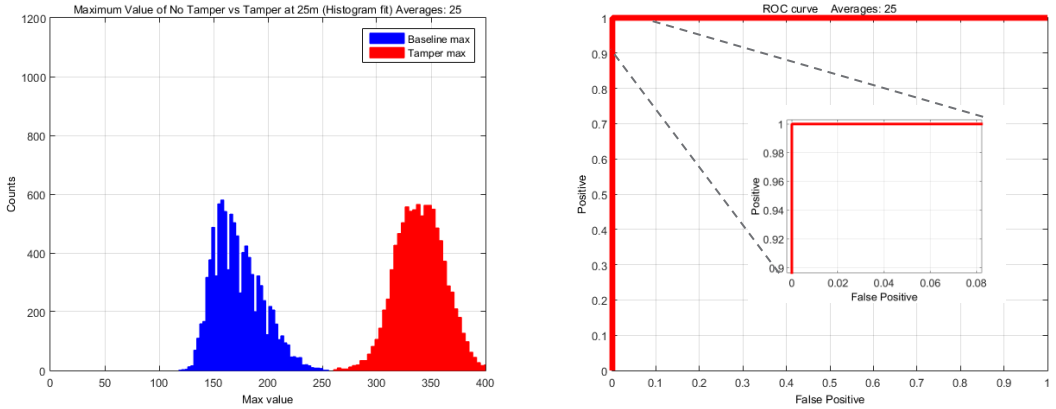

Figure 20. Baseline (blue) and tampered (red) populations (left) and corresponding ROC curve (right) assuming tamper at 25m and averaging of 25 scans per sample.

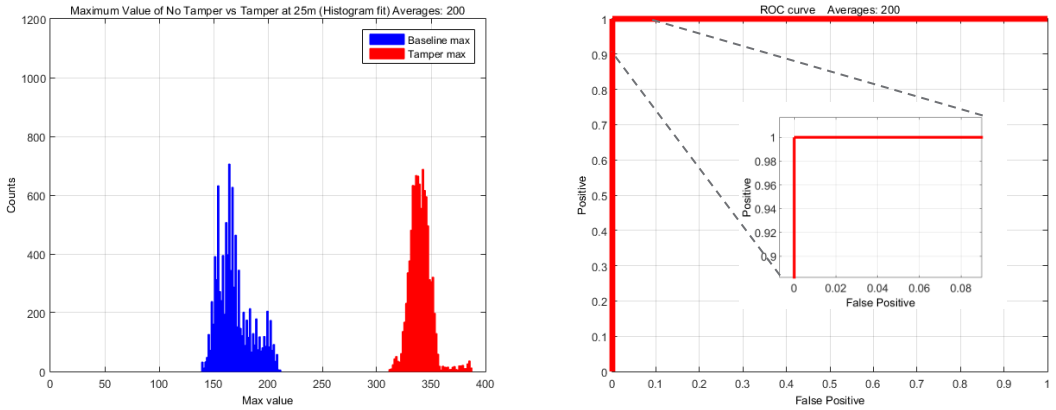

Figure 21. Baseline (blue) and tampered (red) populations (left) and corresponding ROC curve (right) assuming tamper at 25m and averaging of 200 scans per sample.

Figure 19 illustrates that for this particular scenario, expected performance is very poor if no scan averaging is applied. Averaging over 25 scans provides a complete separation of the two histograms and

therefore, perfect ROC performance for this relatively small sample population. Averaging over 200 scans further separates the histograms but does not improve the ROC performance for this proof-of-principle test (with a relatively limited sample population).

Averaging requirements at shorter distances may not be sufficient at longer cable ranges as the attenuation in the cable reduces the dynamic range between the reflected signal and the noise. Figure 22 demonstrates that even with the use of 200-scan averaging, the signal-to-noise ratio for tampers at 37.5m is significantly lower than at 25m, and the ROC curve shows much degraded performance: a FAR of greater than 0.5 is required to achieve PD greater than 0.95. Based on the close proximity of the centroids in the population histograms, it is not clear that a higher degree of scan averaging will produce acceptable performance. Other variables (e.g., transmission power, bandwidth) may need to be modified in order to achieve high-fidelity performance for long cables.

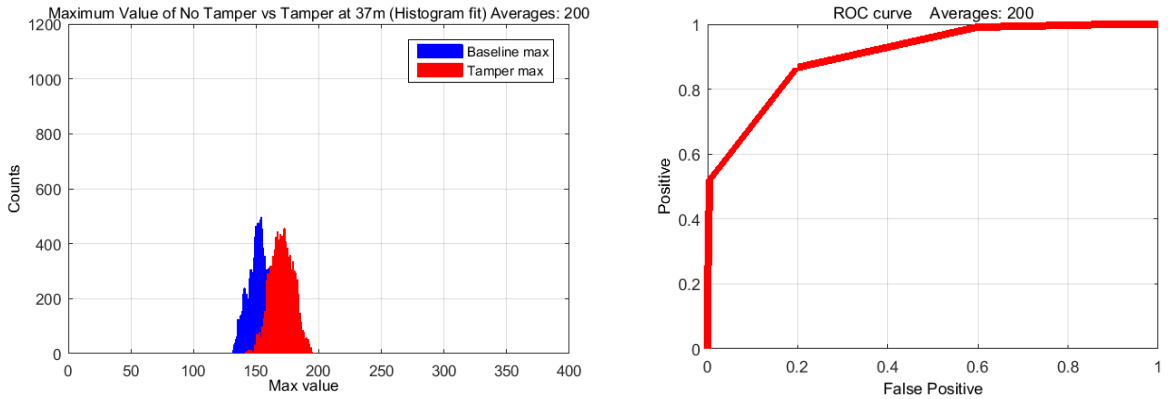

Figure 22. Baseline (blue) and tampered (red) populations (left) and corresponding ROC curve (right) assuming tamper at 37.5m and averaging of 200 scans per sample.

The demonstration case study described above should not be interpreted as a definitive evaluation of LiveWire performance for this scenario. Rather, it serves to illustrate the performance evaluation methods and metrics that PNNL plans to apply to continuing study of candidate TI methods, and accompanying signal analysis algorithms. PNNL's TDR experts and signal-processing experts will collaborate to prioritize the range of parameter settings and algorithms to be considered and evaluated in future work. Among the possibilities are spatially dependent thresholds that recognize the very different noise levels as a function of distance from the interrogation end of the cable. Another is digital filtering in the frequency domain, a possibility discussed below.

7.0 Frequency-Domain Filtering: Proof-of-principle Case Study

As discussed previously, a significant concern with active TDR methods is that the TDR interrogation signal will perturb the radiation sensor signal being collected by the IAEA UMS, and possibly degrade the fidelity of the instrument performance. Rigorous study of this question is a subject of future work but in FY15, an initial inquiry into the topic was performed using frequency-domain digital filtering. As with the proof-of-principle ROC analysis above, the example analysis below is intended to demonstrate that PNNL has the benchtop testing configurations, necessary data collection tools, and analysis expertise to

address the question of signal interference, and to evaluate signal processing methods to mitigate interference effects.

Shown below in Figure 23 is a simple block diagram of the test configuration for this case study, where the LiveWire interrogating pulse was transmitted on the same coaxial cable carrying an AWG signal intended to be representative of a typical IAEA UMS radiation detector, 3.33 MHz single sine wave. In this experiment, data collection was performed using an oscilloscope for: a) only the LiveWire SSTDR, b) only the AWG, and c) both LiveWire and the AWG transmitting simultaneously and therefore, intermodulated. Examples of these three data streams are given in Figure 24.

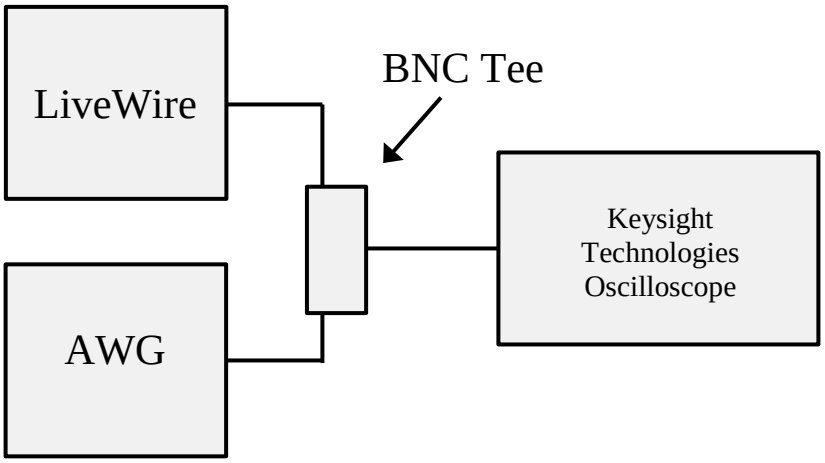

Figure 23. Test configuration for case study on potential interference between LiveWire TDR and signals representative of radiation sensors used in IAEA UMS, here approximated using an AWG.

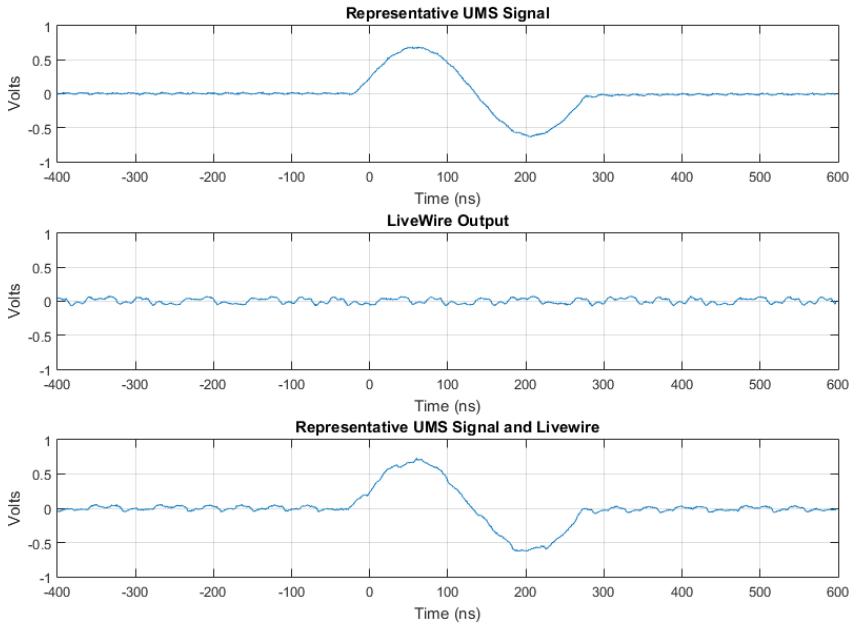

Figure 24. Oscilloscope traces (time domain) for: Sensor, Livewire TDR, and combined signals.

The Fourier transform of the time-domain signals were calculated in order to compare the frequency content of each signal. The frequency-domain signals are depicted in Figure 25 below. Note that the vertical scale for the LiveWire output is changed in order to highlight the frequency structure.

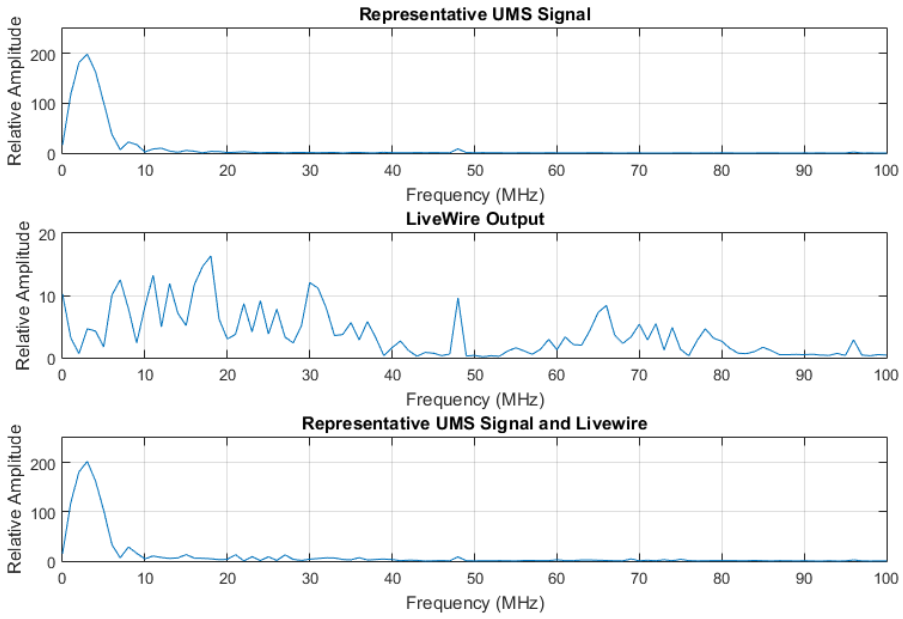

Figure 25. Frequency spectra for sensor, Livewire TDR, and combined signals

Based on the desired frequency range of the sensor signal, a digital lowpass filter (LPF) was applied to the combined signal with the goal of rejecting the high-frequency noise induced on the sensor signal by the TDR interrogation pulse. After applying this LPF in the frequency domain, the inverse Fourier transform is used to bring the data back into the time domain, in a form suitable for IAEA UMS data computation. An example of the unfiltered combined signal, and the filtered combined signal is shown in Figure 26 below.

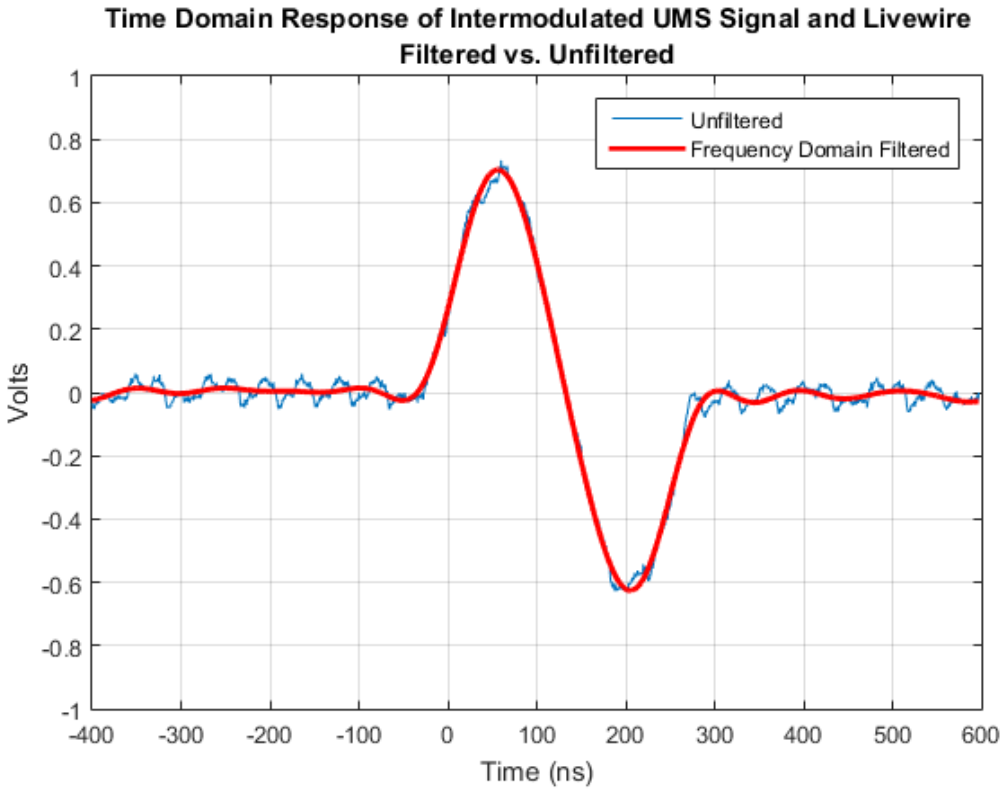

Figure 26. Time-domain response for the unfiltered (blue) and filtered (red) sensor signal.

The simple experiment described above is just one example of the type of digital filtering techniques that could be applied to the active TDR methods. Future work will prioritize the investigations expected to be most fruitful for the IAEA's UMS systems and deployment scenarios.

8.0 Summary and Next Steps

PNNL has developed a test bed on which to base an exploration of two candidate active TDR methods, for monitoring the physical integrity of cabling in unattended radiation detection systems. The laboratory-grade VNA (SFTDR) method is capable of interrogating a wide range of frequencies and pulse structures, while the relatively low-cost commercially available implementation of SSTDR from LiveWire has a more restricted range of operation. The initial findings from a preliminary comparison of the two methods are that both methods show similar trends in terms of intrusion detectability, and that for the specific SFTDR and SSTDR parameters investigated to date, the LiveWire signals provide greater contrast to a reference baseline. It is important to note, however, that the VNA system and frequency range utilized in these initial tests are not optimal for IAEA's unattended radiation-detector scenarios

(e.g., strong attenuation of higher frequencies in long cable length). Future work should employ a VNA with a lower frequency range (e.g., 100 kHz to a few GHz) that is better matched to this application. Also, the LiveWire analysis presented here was based on the averaging of 200 scans, as compared to the VNA's single scan. A definitive comparison of the methods will required data acquisition and analysis methods that provide a more level playing field for the two candidate methods.

In FY15, PNNL defined, developed and demonstrated a performance metric based on ROC curves. ROC analysis was deemed well-suited to IAEA UMS applications because it quantifies the unavoidable tradeoffs between detection probability and false alarms, and allows direct comparison of performance in very different scenarios (defined, for example, by electromagnetic noise levels, cable lengths, etc.). PNNL also demonstrated the benchtop test configuration, data collection methods and signal analysis toolbox that can support investigation of signal interference and digital filtering techniques in the frequency domain.

PNNL's FY15 progress sets the stage for a thorough investigation of LiveWire as it might be implemented by the IAEA, and comparison of that COTS TDR method to a gold-standard benchtop TDR method. That evaluation will be based on the cable tampering scenarios and detection objectives defined previously by the NGSI project team. The next steps along that path would include:

- Task 1: Complete comparative evaluation of LiveWire against a benchtop gold-standard TDR method using scenarios and metrics previously defined.
- Task 2: Design and fabricate prototype TDR device based on findings of Task 1 and if necessary, adaptations of the LiveWire ASIC, in collaboration with LiveWire.
    - Optimal hardware and software configurations
    - Determine digital signal processing techniques to improve TDR sensor detection and isolate TDR from UMS signals.
- Task 3: Prototype testing and demonstration with representative UMS sensors and data acquisition systems (available from previous NGSI and PNNL internal investments), and in realistic environments.

9.0 References

[1]Tedeschi JR, Smith LE, Moore DE, Sheen DM, Conrad RC. 2014. *Active Time Domain Reflectometry for Tamper Indication in Unatted Monitoring Systems for Safeguards*. PNNL – 23893, Pacific Northwest National Laboratory, Richland, Washington.

[2]Smith LE, Svoboda J, Ianakiev K, et al. 2014. " Front-end electronics for verification measurements: performance evaluation and viability of advanced tamper indicating measures." IAEA International Safeguards Symposium.

[3]Smith LE, P Ramuhalli, DM Sheen, JR Tedeschi, RC Conrad, K Ianakiev, M Browne, J Svoboda, J West and J Sanders. 2014. *Detection of Physical Intrusion in the Cabling of Unattended Safeguards Instruments: Preliminary Requirements and Evaluation Scenarios*. PNNL-23749, Pacific Northwest National Laboratory, Richland, Washington.

[4]Keysight Technologies. 2014. *Keysight Electronic Calibration (ECal) Modules for Vector Network Analyzers - Technical Overview*. Keysight Technologies, Inc. Santa Rose, California. Accessed November 11, 2014. Available at http://literature.cdn.keysight.com/litweb/pdf/5963-3743E.pdf.

[5]Agilent. 2012. *Time Domain Analysis Using a Network Analyzer*. Application Note 1287-12, Agilent Technologies, Santa Clara, California. Available at http://cp.literature.agilent.com/litweb/pdf/5989-5723EN.pdf.

[6]Wadell BC. 1991. "Transmission Line Handbook" Norwood, MA: Artech House Inc.

[7]LiveWire. 2014. *Live Cable Fault Monitoring*. LiveWire Innovation. South Jordan, Utah. Accessed November 11, 2014. http://LiveWireinnovation.com/.

[8]Smith P, C Furse and J Gunther. 2005. "Analysis of Spread Spectrum Time Domain Reflectometry for Wire Fault Location." *IEEE Sensors Journal* 5(6):1469-1478.

[9]IAEA. 2013. *IAEA Department of Safeguards Long-Term R&D Plan, 2012-2023*. STR-375, International Atomic Energy Agency (IAEA), Vienna, Austria.

[10]Wellshow. 2015. *RG-174 Coaxial Cable*, Taoyuan City, Taiwan. Accessed May 25, 2015, http://www.wellshow.com/.

Appendix A

FY15 TDR Measurement List

Appendix A

FY15 TDR Measurement List

FEUM Measurement List 4/24/15							
Non-Destructive Testing							
Measurement System	Cable Type	Cable Length	Tamper/Impedance Description	Tamper/Impedance change location	Measurement Configuration #	File Name	Folder
Power: 32 mV							
LiveWire	RG174	50m	50Ohm Termination (BASELINE)	50m	1	032mV_Base.csv	\\pnl\projects\FEUM\People\Gavric\04_2015_FEUM_tests\Livewire\50m_24Mhz_32mV
LiveWire	RG174	50m	30dB pad at end of cable	50m	1	032mV_30dB.csv	""
LiveWire	RG174	50m	20dB pad at end of cable	50m	1	032mV_20dB.csv	""
LiveWire	RG174	50m	10dB pad at end of cable	50m	1	032mV_10dB.csv	""
LiveWire	RG174	50m	8dB pad at end of cable	50m	1	032mV_08dB.csv	""
LiveWire	RG174	50m	6dB pad at end of cable	50m	1	032mV_06dB.csv	""
LiveWire	RG174	50m	3dB pad at end of cable	50m	1	032mV_03dB.csv	""
LiveWire	RG174	50m	2dB pad at end of cable	50m	1	032mV_02dB.csv	""
LiveWire	RG174	50m	1dB pad at end of cable	50m	1	032mV_01dB.csv	""
LiveWire	RG174	50m	OPEN at cable end	50m	1	032mV_Open.csv	""
LiveWire	RG174	50m	SHORT at cable end	50m	1	032mV_Short.csv	""
Power: 64 mV							
LiveWire	RG174	50m	50Ohm Termination (BASELINE)	50m	1	064mV_Base.csv	z_64mV
LiveWire	RG174	50m	30dB pad at end of cable	50m	1	064mV_30dB.csv	""
LiveWire	RG174	50m	20dB pad at end of cable	50m	1	064mV_20dB.csv	""
LiveWire	RG174	50m	10dB pad at end of cable	50m	1	064mV_10dB.csv	""
LiveWire	RG174	50m	8dB pad at end of cable	50m	1	064mV_08dB.csv	""
LiveWire	RG174	50m	6dB pad at end of cable	50m	1	064mV_06dB.csv	""
LiveWire	RG174	50m	3dB pad at end of cable	50m	1	064mV_03dB.csv	""
LiveWire	RG174	50m	2dB pad at end of cable	50m	1	064mV_02dB.csv	""
LiveWire	RG174	50m	1dB pad at end of cable	50m	1	064mV_01dB.csv	""
LiveWire	RG174	50m	OPEN at cable end	50m	1	064mV_Open.csv	""
LiveWire	RG174	50m	SHORT at cable end	50m	1	064mV_Short.csv	""
Power: 128 mV							
LiveWire	RG174	50m	50Ohm Termination (BASELINE)	50m	1	128mV_Base.csv	\\pnl\projects\FEUM\People\Gavric\04_2015_FEUM_tests\Livewire\50m_24Mhz_128mV
LiveWire	RG174	50m	30dB pad at end of cable	50m	1	128mV_30dB.csv	""
LiveWire	RG174	50m	20dB pad at end of cable	50m	1	128mV_20dB.csv	""
LiveWire	RG174	50m	10dB pad at end of cable	50m	1	128mV_10dB.csv	""
LiveWire	RG174	50m	8dB pad at end of cable	50m	1	128mV_08dB.csv	""
LiveWire	RG174	50m	6dB pad at end of cable	50m	1	128mV_06dB.csv	""
LiveWire	RG174	50m	3dB pad at end of cable	50m	1	128mV_03dB.csv	""
LiveWire	RG174	50m	2dB pad at end of cable	50m	1	128mV_02dB.csv	""
LiveWire	RG174	50m	1dB pad at end of cable	50m	1	128mV_01dB.csv	""
LiveWire	RG174	50m	OPEN at cable end	50m	1	128mV_Open.csv	""
LiveWire	RG174	50m	SHORT at cable end	50m	1	128mV_Short.csv	""
Power: 256 mV							
LiveWire	RG174	50m	50Ohm Termination (BASELINE)	50m	1	256mV_Base.csv	\\pnl\projects\FEUM\People\Gavric\04_2015_FEUM_tests\Livewire\50m_24MHz_256mV
LiveWire	RG174	50m	30dB pad at end of cable	50m	1	256mV_30dB.csv	""
LiveWire	RG174	50m	20dB pad at end of cable	50m	1	256mV_20dB.csv	""
LiveWire	RG174	50m	10dB pad at end of cable	50m	1	256mV_10dB.csv	""
LiveWire	RG174	50m	8dB pad at end of cable	50m	1	256mV_08dB.csv	""
LiveWire	RG174	50m	6dB pad at end of cable	50m	1	256mV_06dB.csv	""
LiveWire	RG174	50m	3dB pad at end of cable	50m	1	256mV_03dB.csv	""
LiveWire	RG174	50m	2dB pad at end of cable	50m	1	256mV_02dB.csv	""
LiveWire	RG174	50m	1dB pad at end of cable	50m	1	256mV_01dB.csv	""
LiveWire	RG174	50m	OPEN at cable end	50m	1	256mV_Open.csv	""
LiveWire	RG174	50m	SHORT at cable end	50m	1	256mV_Short.csv	""
Power: 512 mV							
LiveWire	RG174	50m	50Ohm Termination (BASELINE)	50m	1	512mV_Base.csv	\\pnl\projects\FEUM\People\Gavric\04_2015_FEUM_tests\Livewire\50m_24MHz_512mV
LiveWire	RG174	50m	30dB pad at end of cable	50m	1	512mV_30dB.csv	""
LiveWire	RG174	50m	20dB pad at end of cable	50m	1	512mV_20dB.csv	""
LiveWire	RG174	50m	10dB pad at end of cable	50m	1	512mV_10dB.csv	""
LiveWire	RG174	50m	8dB pad at end of cable	50m	1	512mV_08dB.csv	""
LiveWire	RG174	50m	6dB pad at end of cable	50m	1	512mV_06dB.csv	""
LiveWire	RG174	50m	3dB pad at end of cable	50m	1	512mV_03dB.csv	""
LiveWire	RG174	50m	2dB pad at end of cable	50m	1	512mV_02dB.csv	""
LiveWire	RG174	50m	1dB pad at end of cable	50m	1	512mV_01dB.csv	""
LiveWire	RG174	50m	OPEN at cable end	50m	1	512mV_Open.csv	""
LiveWire	RG174	50m	SHORT at cable end	50m	1	512mV_Short.csv	""
Power: 0 dB							
VNA	RG174	50m	50Ohm Termination (BASELINE)	50m	1	VNA_50m_Base.prn	\\pnl\projects\FEUM\People\Gavric\04_2015_FEUM_tests\VNA\50m_3GHzBW_0dB_5kIF
VNA	RG174	50m	30dB pad at end of cable	50m	1	VNA_50m_30dB.prn	""
VNA	RG174	50m	20dB pad at end of cable	50m	1	VNA_50m_20dB.prn	""
VNA	RG174	50m	10dB pad at end of cable	50m	1	VNA_50m_10dB.prn	""
VNA	RG174	50m	8dB pad at end of cable	50m	1	VNA_50m_08dB.prn	""
VNA	RG174	50m	6dB pad at end of cable	50m	1	VNA_50m_06dB.prn	""
VNA	RG174	50m	3dB pad at end of cable	50m	1	VNA_50m_03dB.prn	""
VNA	RG174	50m	2dB pad at end of cable	50m	1	VNA_50m_02dB.prn	""
VNA	RG174	50m	1dB pad at end of cable	50m	1	VNA_50m_01dB.prn	""
VNA	RG174	50m	OPEN at cable end	50m	1	VNA_50m_Open.prn	""
VNA	RG174	50m	SHORT at cable end	50m	1	VNA_50m_Short.prn	""

Destructive Testing								
Measurement System	Cable Type	Cable Length	Tamper/Impedance Description	Tamper/Impedance change location	Measurement Configuration #	File Name	Folder	Notes
Power: 128 mV								
LiveWire	RG174	50m	50Ohm Termination (BASELINE)	50m	1		\\pnl\projects\FEUM\People\Gavric\05_2015_FEUM_tests\Livewire\Base_end\128mV\csv_data	
LiveWire	RG174	50m	cut through outer conductor, probe penetrating to center conductor	25m	1		\\pnl\projects\FEUM\People\Gavric\05_2015_FEUM_tests\Livewire\Base_end\128mV\csv_data	
LiveWire	RG174	50m	cut through outer conductor, probe penetrating to center conductor	37.5m	1		\\pnl\projects\FEUM\People\Gavric\05_2015_FEUM_tests\Livewire\Base_end\128mV\csv_data	
LiveWire	RG174	50m	cut through outer conductor, probe penetrating to center conductor	50m	1		\\pnl\projects\FEUM\People\Gavric\05_2015_FEUM_tests\Livewire\Base_end\128mV\csv_data	
LiveWire	RG174	50m	AWG at Cable End	50m	2		\\pnl\projects\FEUM\People\Gavric\05_2015_FEUM_tests\Livewire\AWG_end\128mV\csv_data	
LiveWire	RG174	50m	cut through outer conductor, probe penetrating to center conductor	25m	2		\\pnl\projects\FEUM\People\Gavric\05_2015_FEUM_tests\Livewire\AWG_end\128mV\csv_data	
LiveWire	RG174	50m	cut through outer conductor, probe penetrating to center conductor	37.5m	2		\\pnl\projects\FEUM\People\Gavric\05_2015_FEUM_tests\Livewire\AWG_end\128mV\csv_data	
LiveWire	RG174	50m	cut through outer conductor, probe penetrating to center conductor	50m	2		\\pnl\projects\FEUM\People\Gavric\05_2015_FEUM_tests\Livewire\AWG_end\128mV\csv_data	
Power:256 mV								
LiveWire	RG174	50m	50Ohm Termination (BASELINE)	50m	1		\\pnl\projects\FEUM\People\Gavric\05_2015_FEUM_tests\Livewire\Base_end\256mV\csv_data	
LiveWire	RG174	50m	cut through outer conductor, probe penetrating to center conductor	25m	1		\\pnl\projects\FEUM\People\Gavric\05_2015_FEUM_tests\Livewire\Base_end\256mV\csv_data	
LiveWire	RG174	50m	cut through outer conductor, probe penetrating to center conductor	37.5m	1		\\pnl\projects\FEUM\People\Gavric\05_2015_FEUM_tests\Livewire\Base_end\256mV\csv_data	
LiveWire	RG174	50m	cut through outer conductor, probe penetrating to center conductor	50m	1		\\pnl\projects\FEUM\People\Gavric\05_2015_FEUM_tests\Livewire\Base_end\256mV\csv_data	
LiveWire	RG174	50m	AWG at Cable End	50m	2		\\pnl\projects\FEUM\People\Gavric\05_2015_FEUM_tests\Livewire\AWG_end\256mV\csv_data	
LiveWire	RG174	50m	cut through outer conductor, probe penetrating to center conductor	25m	2		\\pnl\projects\FEUM\People\Gavric\05_2015_FEUM_tests\Livewire\AWG_end\256mV\csv_data	
LiveWire	RG174	50m	cut through outer conductor, probe penetrating to center conductor	37.5m	2		\\pnl\projects\FEUM\People\Gavric\05_2015_FEUM_tests\Livewire\AWG_end\256mV\csv_data	
LiveWire	RG174	50m	cut through outer conductor, probe penetrating to center conductor	50m	2		\\pnl\projects\FEUM\People\Gavric\05_2015_FEUM_tests\Livewire\AWG_end\256mV\csv_data	
Power: 512 mV								
LiveWire	RG174	50m	50Ohm Termination (BASELINE)	50m	1		\\pnl\projects\FEUM\People\Gavric\05_2015_FEUM_tests\Livewire\Base_end\512mV\csv_data	
LiveWire	RG174	50m	cut through outer conductor, probe penetrating to center conductor	25m	1		\\pnl\projects\FEUM\People\Gavric\05_2015_FEUM_tests\Livewire\Base_end\512mV\csv_data	
LiveWire	RG174	50m	cut through outer conductor, probe penetrating to center conductor	37.5m	1		\\pnl\projects\FEUM\People\Gavric\05_2015_FEUM_tests\Livewire\Base_end\512mV\csv_data	
LiveWire	RG174	50m	cut through outer conductor, probe penetrating to center conductor	50m	1		\\pnl\projects\FEUM\People\Gavric\05_2015_FEUM_tests\Livewire\Base_end\512mV\csv_data	
LiveWire	RG174	50m	AWG at Cable End	50m	2		\\pnl\projects\FEUM\People\Gavric\05_2015_FEUM_tests\Livewire\AWG_end\512mV\csv_data	
LiveWire	RG174	50m	cut through outer conductor, probe penetrating to center conductor	25m	2		\\pnl\projects\FEUM\People\Gavric\05_2015_FEUM_tests\Livewire\AWG_end\512mV\csv_data	
LiveWire	RG174	50m	cut through outer conductor, probe penetrating to center conductor	37.5m	2		\\pnl\projects\FEUM\People\Gavric\05_2015_FEUM_tests\Livewire\AWG_end\512mV\csv_data	
LiveWire	RG174	50m	cut through outer conductor, probe penetrating to center conductor	50m	2		\\pnl\projects\FEUM\People\Gavric\05_2015_FEUM_tests\Livewire\AWG_end\512mV\csv_data	
Power: -5 dB								
VNA	RG174	50m	50Ohm Termination (BASELINE)	50m	1		\\pnl\projects\FEUM\People\Gavric\05_2015_FEUM_tests\VNA\Base_end\-5dBm	
VNA	RG174	50m	cut through outer conductor, probe penetrating to center conductor	25m	1		\\pnl\projects\FEUM\People\Gavric\05_2015_FEUM_tests\VNA\Base_end\-5dBm	
VNA	RG174	50m	cut through outer conductor, probe penetrating to center conductor	37.5m	1		\\pnl\projects\FEUM\People\Gavric\05_2015_FEUM_tests\VNA\Base_end\-5dBm	
VNA	RG174	50m	cut through outer conductor, probe penetrating to center conductor	50m	1		\\pnl\projects\FEUM\People\Gavric\05_2015_FEUM_tests\VNA\Base_end\-5dBm	
VNA	RG174	50m	AWG at Cable End	50m	2		\\pnl\projects\FEUM\People\Gavric\05_2015_FEUM_tests\VNA\AWG_end\-5dBm	
VNA	RG174	50m	cut through outer conductor, probe penetrating to center conductor	25m	2		\\pnl\projects\FEUM\People\Gavric\05_2015_FEUM_tests\VNA\AWG_end\-5dBm	
VNA	RG174	50m	cut through outer conductor, probe penetrating to center conductor	37.5m	2		\\pnl\projects\FEUM\People\Gavric\05_2015_FEUM_tests\VNA\AWG_end\-5dBm	
VNA	RG174	50m	cut through outer conductor, probe penetrating to center conductor	50m	2		\\pnl\projects\FEUM\People\Gavric\05_2015_FEUM_tests\VNA\AWG_end\-5dBm	

LiveWire Configuration					
Frequency	**3dB Bandwidth**	**#Averages**	**Transmit Power(mV)**	**Psuedo Noise Length**	**VF**
24 Mhz	24 MHz	200	32,64,128,256,512	1023	0.66
VNA Configuration					
Frequency Range	**Transmit Power**	**IF Bandwidth**	**Sweep Speed**		
50 Mhz - 3.05 GHz	0db,-5db	5kHz			

•

www.pnnl.gov

Pacific Northwest
NATIONAL LABORATORY

Proudly Operated by **Battelle** *Since 1965*

U.S. DEPARTMENT OF
ENERGY

902 Battelle Boulevard
P.O. Box 999
Richland, WA 99352
1-888-375-PNNL (7665)